IMG-GCN: Interpretable Modularity-Guided Structure-Function Interactions Learning for Brain Cognition and Disorder Analysis

Jing Xia[1], Yi Hao Chan[1], Deepank Girish[1], Jagath C. Rajapakse[1(✉)]

[1] School of Computer Science and Engineering, Nanyang Technological University, Singapore, Singapore
{jing_xia,yihao.chan,deepank002,asjagath}@ntu.edu.sg

Abstract. Brain structure-function interaction is crucial for cognition and brain disorder analysis, and it is inherently more complex than a simple region-to-region coupling. It exhibits homogeneity at the modular level, with regions of interest (ROIs) within the same module showing more similar neural mechanisms than those across modules. Leveraging modular-level guidance to capture complex structure-function interactions is essential, but such studies are still scarce. Therefore, we propose an interpretable modularity-guided graph convolution network (IMG-GCN) to extract the structure-function interactions across ROIs and highlight the most discriminative interactions relevant to fluid cognition and Parkinson's disease (PD). Specifically, we design a modularity-guided interactive network that defines modularity-specific convolution operation to learn interactions between structural and functional ROIs according to modular homogeneity. Then, an MLP-based attention model is introduced to identify the most contributed interactions. The interactions are inserted as edges linking structural and functional ROIs to construct a unified combined graph, and GCN is applied for final tasks. Experiments on HCP and PPMI datasets indicate that our proposed method outperforms state-of-the-art multi-model methods in fluid cognition prediction and PD classification. The attention maps reveal that the frontoparietal and default mode structures interacting with visual function are discriminative for fluid cognition, while the subcortical structures interacting with widespread functional modules are associated with PD.

Keywords: Brain structure-function interaction · Modularity · Graph convolution network · Attention · Cognition · Brain disorder.

1 Introduction

Brain functional connectivity (FC) illustrates temporal dependency patterns between regional blood-oxygenation-level-dependent signals, measured through resting-state functional MRI (rs-fMRI), while brain structural connectivity (SC) represents the integrity of regional white matter pathways estimated from diffusion MRI (dMRI). Previous studies suggest that FC tends to be strongest

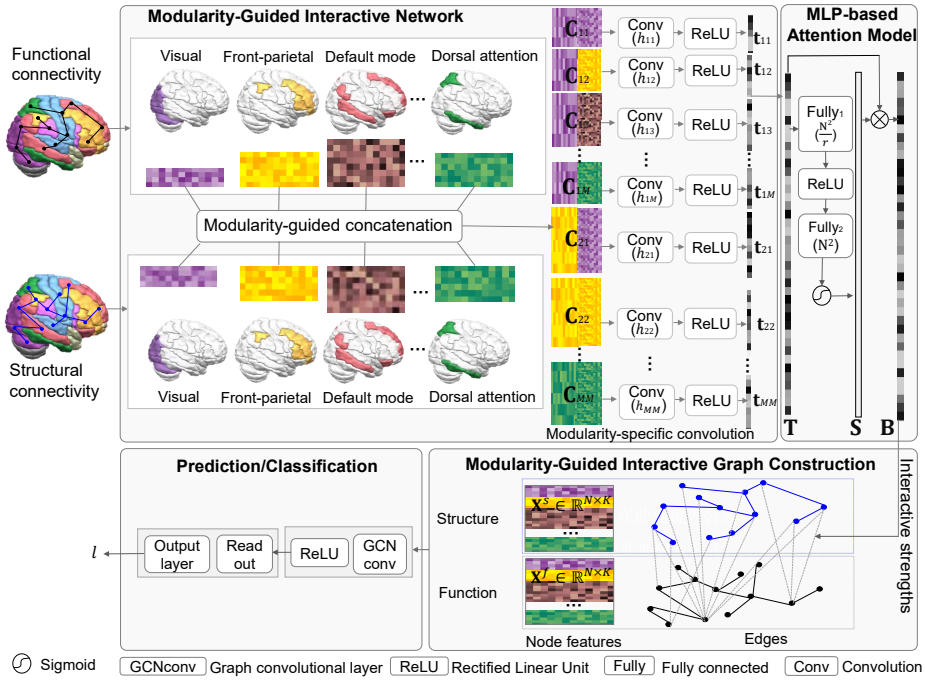

Fig. 1. The overall framework of IMG-GCN involves a modularity-guided interactive network that utilizes FC and SC to define modularity-specific convolution operations, capturing interactions across ROIs. Next, an MLP-based attention model is employed to learn the salient interactions. A modularity-guided interactive graph is constructed by integrating the interactive strengths with the original SC and FC matrices. Subsequently, the graph convolution network utilizes the newly constructed graph for downstream tasks, including prediction and classification.

among regions that are structurally connected [1, 2]. Alterations in the structure-function relationship have been associated with changes in cognition [3, 4] and brain disorders [5, 6]. However, most functional connections are formed without a direct structural link [7]. Therefore, structure-function interaction is likely more complex than a simple correspondence between paired regions of two modalities [8]. High-order interactions across brain regions give rise to complex mappings between structure and function [9]. Understanding these interactions across regions can provide insight into the underlying structural foundation provided by white-matter fiber tracts for brain function, and facilitate the detection of subtle disruptions in brain connectivity that are more sensitive than using a single modality, ultimately enhancing analyses of cognition and brain disorders.

The human brain is organized as a modular system [10], with a set of regions of interest (ROIs) in each module that is less connected to ROIs in other modules while highly interconnected within the module [11]. One typical modular system divides the whole brain into distinct modules based on similar functional or structural foundations, including visual, frontoparietal, default mode, dorsal at-

tention, ventral attention, somatomotor, and limbic modules [12]. At the modular level, structure-function interaction demonstrates homogeneity [13], with ROIs within the same module exhibiting more similar neural mechanisms of structure-function coupling than those across modules. Therefore, leveraging the modular level guidance to capture the complex structure-function interactions has more biological meaning, but it is often overlooked in existing studies.

Based on this, we propose an interpretable modularity-guided graph convolution network (IMG-GCN) to extract complex structure-function interactions, guided by modular homogeneity, while capturing salient interactions relevant to cognition and brain disorders, as shown in Fig. 1. In IMG-GCN, we design a novel modularity-guided interactive network for learning the cross-ROI interactive strengths between two modalities through a modularity-specific convolution operation, which simulates the coupling process across modules. A higher interactive strength represents a stronger coupling relationship between structure and function. Then, a bottleneck-like multilayer perception (MLP)-based attention model is employed to highlight the interactions that contribute most to tasks through attention weights. By inserting the learned interactive strengths as edges connecting all regions between SC and FC, we construct a unified graph and use GCN for final tasks. To evaluate the effectiveness of IMG-GCN, we conduct experiments for fluid cognition prediction and Parkinson's disease (PD) classification. Experiments demonstrate that IMG-GCN outperforms SVM and five state-of-the-art competing graph-based methods based on FC and SC. Furthermore, IMG-GCN provides interpretable attention maps revealing that large-scale structure-function interactions, especially the frontoparietal and default mode structures interacting with visual function, are discriminative for fluid cognition prediction, whereas abnormal brain subcortical structures interacting with widespread functional modules are most discriminative for PD.

2 Materials and Methodology

2.1 Datasets and Image Preprocessing

For fluid cognition prediction, we used a dataset of 838 participants from the Human Connectome Project (HCP) [14]. For PD classification, we used the Parkinson's Progressive Markers Initiative (PPMI) [15] dataset consisting of 69 normal controls and 72 patients with PD. Both datasets include corresponding T1w, rs-fMRI, and dMRI images. For HCP, rs-fMRI and dMRI images were preprocessed by the DPARSF 5.1 advanced toolkit and brain diffusion toolkit within the FSL toolbox [16], respectively. For PPMI, rs-fMRI and dMRI images were preprocessed by fMRIPrep [17] and Clinica [18]. FC and SC were constructed with 116 ROIs, following the Anatomical Automatic Labeling (AAL) protocol [19], including both cortical and subcortical structures. Fluid cognition scores were extracted from the Fluid Cognition Composite (CogFluidComp) in the phenotype list of the HCP dataset, ranging from 87 to 147. Functional connectivity between paired ROIs was computed using the Pearson correlation coefficient. A modified version of Yeo 7-network parcellation [12] was used for both structural

and functional modular systems. It was modified by introducing an additional subcortical module, thus 8 modules were considered in our study.

2.2 Proposed Method

As shown in Fig. 1, the proposed IMG-GCN consists of (1) modularity-guided interactive network, (2) MLP-based attention model, and (3) modularity-guided interactive graph construction, with details introduced below.

Graph Representation The brain connectome can be naturally modeled as a graph with brain ROIs as nodes and the connectivity between these ROIs as edges. For each participant, a functional connectivity graph $\mathbf{G}^f = (\mathbf{V}^f, \mathbf{A}^f, \mathbf{X}^f)$ is constructed. $\mathbf{A}^f \in \mathbb{R}^{N\times N}$ represents the adjacency matrix, defined as thresholded functional connectivity matrix with preserving the highest 10% edges [20] for each node to maintain its connection sparsity. $\mathbf{X}^f = \{\mathbf{x}_1^f, \mathbf{x}_2^f, ..., \mathbf{x}_N^f\} \in \mathbb{R}^{N\times K}$ represents the features of N nodes, and $\mathbf{x}_n^f$ is the feature of node n with length K. Similarly, a structural connectivity graph $\mathbf{G}^s = (\mathbf{V}^s, \mathbf{A}^s, \mathbf{X}^s)$ is constructed. Note that $\mathbf{V}^s$ and $\mathbf{V}^f$ are the same sets of ROIs. $\mathbf{A}^s \in \mathbb{R}^{N\times N}$ denotes the adjacency matrix derived from dMRI, and $\mathbf{X}^s = \{\mathbf{x}_1^s, \mathbf{x}_2^s, ..., \mathbf{x}_N^s\} \in \mathbb{R}^{N\times K}$ is the features of N nodes. For each node in $\mathbf{G}^f$ or $\mathbf{G}^s$, its node feature is defined as the connectivity with all other nodes, respectively.

Modularity-Guided Interactive Network In this network, we capture cross-ROI interactions between structure and function guided by the brain modular system. The whole brain consists of M modules, where the module i contains N_i ROIs, and $\sum_{i=1}^{M} N_i = N$. Given $\mathbf{X}^s$ and $\mathbf{X}^f$, we concatenate the functional node feature of every ROI in module i and the structural node feature of every ROI in module j row by row, achieving the modularity-specific feature $\mathbf{C}_{ij} = \begin{bmatrix} \mathbf{x}_{i,1}^f & \mathbf{x}_{j,1}^s \\ \mathbf{x}_{i,1}^f & \mathbf{x}_{j,2}^s \\ \vdots & \vdots \\ \mathbf{x}_{i,N_i}^f & \mathbf{x}_{j,N_{j-1}}^s \\ \mathbf{x}_{i,N_i}^f & \mathbf{x}_{j,N_j}^s \end{bmatrix} \in \mathbb{R}^{N_i N_j \times 2K}, i, j \in [1, M]$. Here, $\mathbf{x}_{i,1}^f$ means the functional node feature of the first ROI in module i, and $\mathbf{x}_{j,1}^s$ means the structural node feature of the first ROI in module j. After concatenation, we achieve M^2 modularity-specific features. For each feature $\mathbf{C}_{ij}$, we define a modularity-specific convolution operation with a filter h_{ij}, whose kernel size is $1 \times 2K$, followed by one rectified linear unit (ReLU), as

$$\mathbf{t}_{ij} = ReLU(\mathbf{C}_{ij} * h_{ij}) \in \mathbb{R}^{N_i N_j \times 1}, i, j \in [1, M], \tag{1}$$

where $*$ denotes the convolution operation. $\mathbf{t}_{ij}$ represents the interactions between all functional ROIs in module i and structural ROIs in module j. Our hypothesis posits that ROIs within the same module of each modality exhibit

more similar neural mechanisms of structure-function coupling than those across modules. Guided by this coupling homogeneity within modules and heterogeneity across modules, we define M^2 convolution filters for M^2 modularity-specific features. The cross-ROI interactions of the whole brain $\mathbf{T}$ is a concatenation of those of all modules, as $\mathbf{T} = [\mathbf{t}_{11}; \mathbf{t}_{12}; ...; \mathbf{t}_{ij}; ...; \mathbf{t}_{MM}] \in \mathbb{R}^{N^2 \times 1}, i, j \in [1, M]$.

MLP-based Attention Model To identify the most relevant interactions for prediction or classification, we introduce an attention mechanism inspired by an existing squeeze-and-excitation network [21]. Recalling the interactions $\mathbf{T}$, we use a bottleneck-like MLP with two fully connected layers, one ReLU, and one sigmoid activation to define the attention map $\mathbf{S} \in \mathbb{R}^{N^2 \times 1}$ as,

$$\mathbf{S} = Sigmoid\Big[Fully_2\Big(ReLU\big(Fully_1(\mathbf{T})\big)\Big)\Big]. \tag{2}$$

$\mathbf{S}$ identifies the interactions that contribute the most to the task. A higher attention value in $\mathbf{S}$ indicates a greater contribution of the interaction to the task. The first fully connected layer reduces the spatial dimension from N^2 rows to $\frac{N^2}{r}$ hidden nodes, and the second fully connected layer recalibrates N^2 rows from $\frac{N^2}{r}$ hidden nodes, where r is the bottleneck ratio of the fully connected layers. The output of the attention model is defined as $\mathbf{B} = \mathbf{T} \otimes \mathbf{S}$, where $\otimes$ indicates element-wise multiplication. Through this multiplication, interactions that contribute most to outcomes are enhanced, while those that contribute least are suppressed. $\mathbf{B}$ can be reshaped into an $N \times N$ matrix, representing the interactive strengths between N structural nodes and N functional nodes.

Modularity-Guided Interactive Graph Construction Instead of simply combining two graphs, we merge $\mathbf{G}^s$ and $\mathbf{G}^f$ into a unified graph $\mathbf{G} = (\mathbf{V}, \mathbf{A}, \mathbf{X})$, encoding high-order structure-function interactions. The total node set $\mathbf{V} = \begin{bmatrix}\mathbf{V}^s \\ \mathbf{V}^f\end{bmatrix}$ has a size of $2N$, and accordingly, the node feature matrix is set as $\mathbf{X} = \begin{bmatrix}\mathbf{X}^s \\ \mathbf{X}^f\end{bmatrix} \in \mathbb{R}^{2N \times K}$. To interlink $\mathbf{V}^s$ and $\mathbf{V}^f$ across nodes, we insert the interactive strength matrix $\mathbf{B}$ as $N \times N$ edges connecting nodes in $\mathbf{V}^s$ and $\mathbf{V}^f$. The new adjacency matrix is $\mathbf{A} = \begin{bmatrix}\mathbf{A}^s, \mathbf{B} \\ \mathbf{B}, \mathbf{A}^f\end{bmatrix} \in \mathbb{R}^{2N \times 2N}$. Using this integration, the structural and functional profiles associated with all ROIs are allowed to interact, enabling analysis of the unified graph through a single graph convolutional layer as $\mathbf{Z} = GCN(\mathbf{A}, \mathbf{X}) = ReLU(\overline{\mathbf{A}}\mathbf{X}\mathbf{W})$. Here, $\mathbf{W}$ defines the convolution weights for the unified graph. Finally, we use a readout layer employing the flattening method on $\mathbf{Z}$, followed by an output layer consisting of one fully connected layer with dropout and ReLU, and another fully connected layer to generate the outcome. Note that, the loss function is defined as RMSE between the output and true values for the prediction task, and cross-entropy for the classification task.

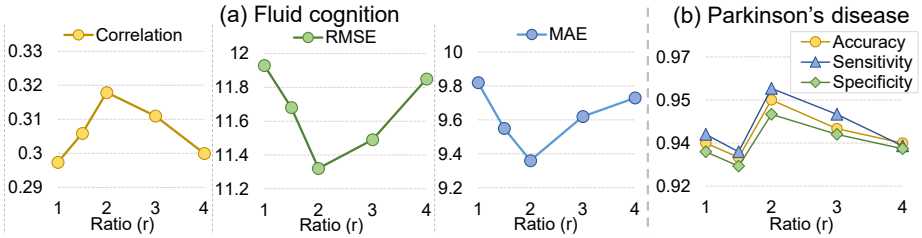

Fig. 2. The results of (a) fluid cognition prediction and (b) PD classification changes with different bottleneck ratios in the MLP-based attention model.

Implementations IMG-GCN was implemented in PyTorch and trained using an Adam optimizer, with learning rates set to 0.0005 for prediction and 0.0001 for classification, and training epochs set to 20 for prediction and 30 for classification. We conducted 5-fold cross-validation to validate model performance. We ran 10 runs of cross-validation and reported average and standard deviation of cross-validation accuracies. Pearson's correlation coefficient, root mean square error (RMSE), and mean absolute error (MAE) were employed to evaluate prediction performance, while accuracy, sensitivity, and specificity were used to quantify classification performance. To avoid overfitting, we used dropout layers after the readout layer and between two fully connected layers in the output layer. Moreover, we adopted L2 regularization with a weight setting of 0.001 to prevent overfitting.

3 Experiments and Results

Competing Methods and Hyperparameter Setting We comprehensively compared IMG-GCN against a shallow method SVM (feeding the upper matrices of the FC and SC together into the classifiers) and five state-of-the-art methods based on brain FC and SC to predict fluid cognition and classify patients with PD. Specifically, **M-GCN** [22], **HGNN** [23] and **MV-GCN** [24] combined the structure and function features for tasks without utilization of interactions, whereas **Cross-GNN** [25] and **Joint-GCN** [26] utilized the interactions between paired regions of two modalities without modular information. In our IMG-GCN, N and K equal to 116, and M equals to 8. The bottleneck ratio (r) in the MLP was set to 2 based on the optimal performance observed in Fig. 2. The output layer comprised two fully connected layers with 256 and 1 hidden nodes for prediction, as well as 256 and 2 hidden nodes for classification. The dropout rate was set at 0.5. We adjusted hyperparameters for competing methods to suit our application. In M-GCN and HGNN, all hyperparameters were set as in [22] and [23]. In MV-GCN, three fully connected layers were set with 1024, 64, and 1 hidden nodes, respectively. For Cross-GNN, the feature dimensions of GCN were set as 64. In Joint-GCN, three fully connected layers were set with 3712, 256, and 1 hidden nodes. Other hyperparameters and learning rates were set based on their original publications. RMSE and cross-entropy

were adopted as the loss functions for prediction and classification, respectively. For classification, the last fully connected layer was set with 2 hidden nodes.

Comparison with Competing Methods Table 1 demonstrated the comparison results on HCP and PPMI datasets, listing the mean and standard deviation of ten runs. All GCN-based methods generally outperformed the SVM method, which relies on handcrafted node features without graph topological information. Moreover, our IMG-GCN significantly performed better on both tasks than M-GCN, HGNN, and MV-GCN, which do not utilize interactions. Compared with Joint-GCN and Cross-GNN, our method significantly improved correlation by 10% to 14% on the fluid cognition prediction and accuracy by 2% to 6% on the PD classification, respectively. We inferred these improvements were attributed to capturing meaningful complex interactions between structural ROIs and functional ROIs guided by modular homogeneity.

Table 1. Results of seven methods on HCP and PPMI based on FC and SC.

Methods	Fluid cognition prediction			Parkinson's disease classification		
	Correlation	RMSE	MAE	Accuracy	Sensitivity	Specificity
SVM	0.24(0.03)∗	13.19(0.95)∗	11.89(0.67)∗	0.76(0.09)∗	0.77(0.09)∗	0.73(0.08)∗
M-GCN	0.26(0.02)∗	12.63(0.68)∗	11.15(0.72)∗	0.90(0.05)∗	0.88(0.06)∗	0.91(0.06)∗
HGNN	0.26(0.03)∗	12.74(1.01)∗	11.27(0.86)∗	0.82(0.06)∗	0.84(0.08)∗	0.80(0.07)∗
MV-GCN	0.27(0.03)∗	12.18(0.86)∗	10.34(0.97)∗	0.92(0.06)∗	0.92(0.05)∗	0.91(0.08)∗
Cross-GNN	0.28(0.02)∗	11.95(0.82)∗	10.08(0.66)∗	0.93(0.07)∗	0.94(0.08)	0.93(0.09)
Joint-GCN	0.29(0.01)∗	11.78(0.89)∗	9.87(0.74)∗	0.90(0.12)∗	0.92(0.09)∗	0.87(0.11)∗
Ours	**0.32(0.02)**	**11.27(0.75)**	**9.36(0.79)**	**0.95(0.06)**	**0.95(0.06)**	**0.94(0.07)**

'*' indicates the results of IMG-GCN and the competing method are significantly different, confirmed by the student's t-test (p¡0.05).

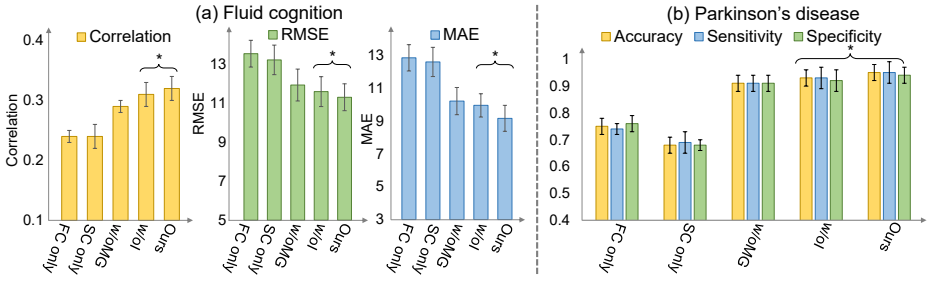

Fig. 3. Results of the ablation study of IMG-GCN, comparing with five degenerated variants for (a) fluid cognition prediction and (b) PD classification. The term '*' indicates the results of IMG-GCN and the degenerated variant are significantly different, confirmed by the student's t-test (p¡0.05).

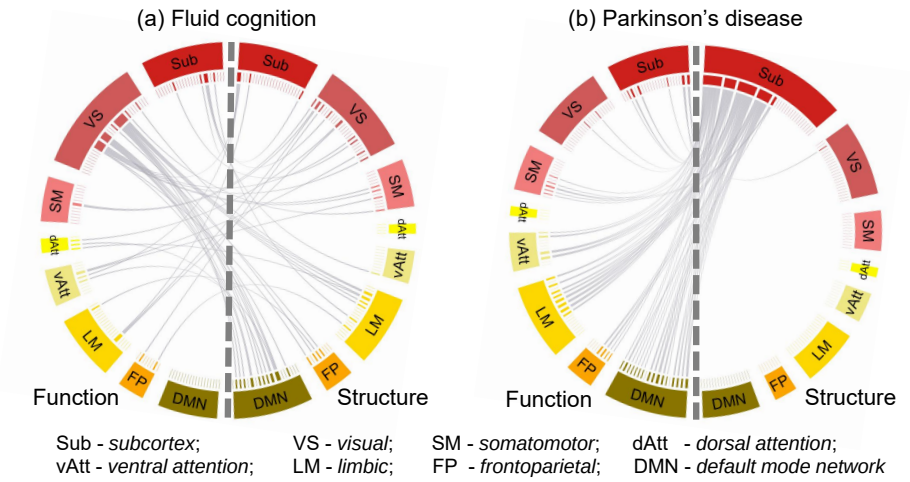

Fig. 4. The top 5% discriminative interactions between structural and functional ROIs identified by the MLP-based attention model were associated with (a) fluid cognition and (b) PD. Specifically, the attention map revealed that large-scale interactions contributed to fluid cognition prediction, while abnormal subcortical structures interacting with widespread functional modules were the most discriminative for PD classification.

Ablation Study In this experiment, we performed an ablation study to assess the performance of each model. Our first aim was to evaluate the effectiveness of the modularity-guided interactive network, and our second aim was to investigate the significance of utilizing the MLP-based attention model. We compared the proposed IMG-GCN with its five degenerated variants: single GCN performed on 1) uni-modal FC and 2) uni-modal SC; 3) IMG-GCN without the modularity-guided interactive network (all values in $\mathbf{T}$ were set as 0.1) (w/oMG); 4) IMG-GCN without MLP-based attention model (w/oI); and 5) IMG-GCN (ours). Fig. 3(a) and 3(b) indicated that our IMG-GCN method significantly achieved the highest correlation and the lowest RMSE and MAE, respectively for prediction, as well as the highest accuracy, sensitivity, and specificity for classification.

Discriminative Structure-Function Interactions The top 5% discriminative structure-function interactions for fluid cognition prediction and PD classification, identified by the attention weights $\mathbf{S}$ from the MLP-based attention model, are shown in Fig. 4. Large-scale structure-function interactions play a crucial role in fluid cognition prediction (see Fig. 4(a)). Specifically, these interactions involve the frontoparietal and the default mode structures, both associated with high-order cognitive processes, interacting with the visual functional module, mainly contributing to the prediction. Integrating visual information and high-order cognition processes facilitates the executive function [27] - a central component of fluid cognition. Variability in the structure-function coupling between the visual and high-order cognition processing modules is related to dif-

ferent fluid cognition states [28]. Thus, our attention model identifies biological meaningful structure-function interactions associated with fluid cognition.

Abnormal interactions in the subcortical structural module widely interacting with functional modules are most discriminative for PD classification (see Fig. 4(b)). Compared with a current study only focusing on cortical structure-function coupling [29], our results provide further insights into biomarkers in the subcortical module for PD. Previous findings have reported that PD is primarily characterized by the loss of dopaminergic cells and atrophy in subcortical regions [30, 31]. Our findings suggest that the subsequent impact of these subcortical structural changes spreads throughout the brain in patients with PD, ultimately resulting in brain dysfunction.

4 Conclusion

We propose an interpretable modularity-guided structure-function interactive learning network for cognition prediction and PD classification. The salient maps identified by the attention model indicate the salient biological meaningful structure-function interactions associated with fluid cognition and PD. Our work can be further applied to datasets related to brain diseases, such as autism and schizophrenia, to identify salient structure-function coupling markers.

Ackwonledgement. Research supported by AcRF Tier-2 grant MOE T2EP20121-0003 of Ministry of Education, Singapore.

Disclosure of Interests. The authors have no competing interests to declare that are relevant to the content of this article.

References

1. Baum, G.L., et al.: Development of structure–function coupling in human brain networks during youth. Proceedings of the National Academy of Sciences **117**(1), 771-8 (2020).
2. Dhamala, E., et al.: Distinct functional and structural connections predict crystallised and fluid cognition in healthy adults. Human brain mapping **42**(10), 3102-18 (2021).
3. Dong, X., et al.: How brain structure–function decoupling supports individual cognition and its molecular mechanism. Human Brain Mapping **45**(2), e26575 (2024).
4. Gu, Z., et al.: Heritability and interindividual variability of regional structure-function coupling. Nature Communications **12**(1), 4894 (2021).
5. Droby, A., et al.: The interplay between structural and functional connectivity in early stage Parkinson's disease patients. Journal of the Neurological Sciences **442**, 120452 (2022).
6. Wang, L., et al.: Optimization of structural connectomes and scaled patterns of structural-functional decoupling in Parkinson's disease. NeuroImage **284**, 120450 (2023).

7. Suárez, L.E., et al.: Linking structure and function in macroscale brain networks. Trends in cognitive sciences **24**(4), 302-15 (2020).
8. Sarwar, T., et al.: Structure-function coupling in the human connectome: A machine learning approach. NeuroImage **226**., 117609 (2021).
9. Seguin, C., Van Den Heuvel, M.P., Zalesky, A.: Navigation of brain networks. Proceedings of the National Academy of Sciences **115**(24), 6297-302 (2018).
10. Sporns, O., Betzel, R.F.: Modular brain networks. Annual review of psychology **67**, 613-40 (2016).
11. Bertolero, M.A., Yeo, B.T., D'Esposito, M.: The modular and integrative functional architecture of the human brain. Proceedings of the National Academy of Sciences **112**(49), E6798-807 (2015).
12. Yeo, B.T., et al.: The organization of the human cerebral cortex estimated by intrinsic functional connectivity. Journal of neurophysiology **106**3, 1125-1165, (2011).
13. Park, H.J., Friston, K.: Structural and functional brain networks: from connections to cognition. Science **342**(6158), 1238411 (2013).
14. Van Essen, D.C., et al.: The WU-Minn human connectome project: an overview. Neuroimage **80**, 62-79 (2013).
15. Marek, K., et al.: The Parkinson progression marker initiative (PPMI). Progress in neurobiology **95**(4), 629-35 (2011).
16. Jenkinson, M., et al.: Fsl. Neuroimage **62**(2), 782-90 (2012).
17. Esteban, O., et al.: fMRIPrep: a robust preprocessing pipeline for functional MRI. Nature methods **16**(1), 111-6 (2019).
18. Routier, A., et al.: An open-source software platform for reproducible clinical neuroscience studies. Frontiers in Neuroinformatics **15**, 689675 (2021).
19. Tzourio-Mazoyer, N., et al.: Automated anatomical labeling of activations in SPM using a macroscopic anatomical parcellation of the MNI MRI single-subject brain. Neuroimage **15**(1), 273-89 (2002).
20. Li, X., et al.: BrainGNN: Interpretable brain graph neural network for fMRI analysis. Medical Image Analysis **74**, 102233 (2021).
21. Hu, J., Shen, L., Sun, G.: Squeeze-and-excitation networks. In: CVPR, pp. 7132-7141 (2018).
22. Dsouza, N.S., et al.: M-GCN: A multimodal graph convolutional network to integrate functional and structural connectomics data to predict multidimensional phenotypic characterizations. In Medical Imaging with Deep Learning, pp. 119-130 (2021).
23. Feng, Y, et al.: Hypergraph neural networks. In AAAI, vol. 33, pp. 3558-3565 (2019).
24. Zhang, X., et al.: Multi-view graph convolutional network and its applications on neuroimage analysis for parkinson's disease. In AMIA Annual Symposium Proceedings, vol. 2018, pp. 1147 (2018).
25. Yang, Y., et al.: Mapping multi-modal brain connectome for brain disorder diagnosis via cross-modal mutual learning. IEEE Transactions on Medical Imaging **43**1, 108-121 (2023).
26. Li, Y., et al.: Joint graph convolution for analyzing brain structural and functional connectome." In MICCAI, pp.231-240 (2022).
27. Rosen, M.L., Amso, D., McLaughlin, K.A.: The role of the visual association cortex in scaffolding prefrontal cortex development: A novel mechanism linking socioeconomic status and executive function. Developmental cognitive neuroscience **39**, 100699 (2019).
28. Feng, G., et al.: Spatial and temporal pattern of structure-function coupling of human brain connectome with development. bioRxiv, (2023).

29. Zarkali, A., et al.: Organisational and neuromodulatory underpinnings of structural-functional connectivity decoupling in patients with Parkinson's disease. Communications biology **4**(1), 86 (2021).
30. Wang, L., et al.: Dopamine depletion and subcortical dysfunction disrupt cortical synchronization and metastability affecting cognitive function in Parkinson's disease. Human Brain Mapping **43**(5), 1598-610 (2022).
31. Menke, R.A., et al.: MRI characteristics of the substantia nigra in Parkinson's disease: a combined quantitative T1 and DTI study. Neuroimage **47**(2), 435-41 (2009).